Electronic Supplementary Material (ESI) for Nanoscale.
This journal is © The Royal Society of Chemistry 2015

Gain and Raman line-broadening with graphene coated diamond-shape nano-antennas

Charilaos Paraskevaidis[1], Tevye Kuykendall[2], Mauro Melli[2], Alexander Weber-Bargioni[2], P. James Schuck[2], Adam Schwartzberg[2], Scott Dhuey[2], Stefano Cabrini[2] and Haim Grebel[1]*

[1] Electronic Imaging Center, NJIT, Newark, NJ 07102; grebel@njit.edu

[2] The Molecular Foundry, Lawrence Berkeley National Laboratory, Berkeley, CA 94720

Supplemental Information

SERS with 633 nm and 532 nm lasers: Based on these and other spectra, we concluded that our graphene was made of mostly 2 layers. When illuminated by a 633 nm laser, the 2D-line was well within the antennas gain curve, situating at λ=760 nm. The data with the 633 nm laser did not exhibit significant signal enhancement (as also seen by the very dim antennas in Fig. 2c in the main text). The data with the 532 nm laser were obtained after the conclusion of the intensity dependent measurements. No apparent damage (namely, no extraordinary D-line) is detected in these data. There is also no additional peak shift(s) or broadening with respect to the reference signal between antennas.

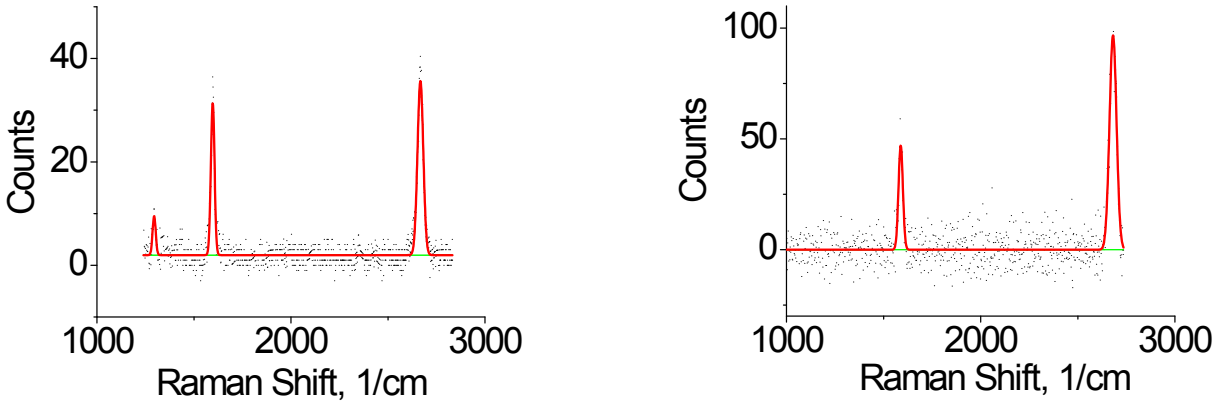

Fig. S1. (a) Fitted Raman spectra of graphene coated D_10_03 antenna taken with a 633 nm laser and polarized in parallel to the antenna's axis (a). The laser frequency is off-resonance but the scattered modes are within the antenna's gain curve. (b) Fitted data of the D_10_07 taken with the 532 nm laser, and polarized along the antenna's axis. The data were taken after the conclusion of the intensity ramp measurements.

Fitting the raw data with the model: The antenna provides gain to all oscillators between the pump and scattered frequencies and the problem becomes nonlinear. The laser light is better absorbed; the Raman signals (and as a matter of fact all other possible oscillators) are better radiating out. We assume that the resonance spectral region may approximate Figure 1c by a line factor, or normalized Lorentzian (namely, a distribution with peak normalized to a constant). The antenna's gain is then written as,

$$G(\varpi) = G_0 \frac{(\sigma_\varpi / 2)^2}{[(\varpi^2 - \varpi_0)^2 + (\sigma_\varpi / 2)^2]}$$

Here, G_0 is the gain amplitude ($G_0 \geq 1$), ϖ_0 is the peak resonance wavenumber and σ_ϖ is the antenna's spectral width. The large field, associated with the antenna resonance is

affecting both the Raman signal and its linewidth. Each of the scattered (Raman) line at ϖ_i may be approximated by a line factor as well,

$$A_i(\varpi) = \frac{c_i \cdot (\Gamma(\varpi)/2)^2}{[(\varpi - \varpi_i + \Delta\varpi)^2 + (\Gamma(\varpi)/2)^2]},$$

where c_i are relative constants of intensity of Raman lines involved. Based on the gain form we approximate the linewidth by, $\Gamma(\varpi) = [1 + G(\varpi)]\Gamma_0$ which implies a large gain for the scattered mode. The small line shift may be attributed to strain, or frequency pulling and is approximated by a small fraction of the spectral width; $\Delta\varpi = a\Gamma_0(\varpi)$. The spectrum of the Raman signal $I(\varpi)$ is the sum of four active Raman lines $A_i(\varpi)$ at approximately 800 (which could be observed between antennas), at ca 1300, 1600 and 2700 cm^{-1} from the laser line. By definition, the relative change in the scattered light intensity equals the gain, $\frac{\delta I(\varpi)}{I(\varpi)} = \gamma(\varpi)$. In turn, this gain is related to the amplified incident field as, $\gamma(\varpi) = N\sigma(\varpi)I_L$. Here, N is the number of graphene atoms involved, $\sigma(\varpi)$ is the Raman scattering cross section peaking at ϖ_i. The cross section at the Raman line $\sigma(\varpi_i)$ and the laser intensity $I_L(\varpi_L)$ are correlated. For narrow Raman line widths, the scattering cross section at the Raman peak is $\sigma(\varpi_i) = \frac{G(\varpi_i)}{G_0} \cdot \sigma_0(\varpi_i)$ and $I_L(\varpi_L) = G(\varpi_L)I_0(\varpi_L)$. Here, σ_0 the scattering cross-section without amplification and I_0 is pump laser intensity. We generalize to all possible oscillators within the antenna gain curve, $\sigma(\varpi) = \frac{G(\varpi)}{G_0} \cdot \sigma_0(\varpi)$. Each scattered component is, thus weighed by a frequency

dependent, antenna gain function. We write for the overall Raman scatterings ($N=\sigma_i=I_L=1$),

$$I(\varpi) = \sum_i A_i(\varpi) \exp[G(\varpi) \cdot G(\varpi_L) / G_0] \cdot$$

In Fig. S2 we show fitting to uncompensated data of Fig. 4c. The increase in spectral background as $\varpi \rightarrow 0$ is a combination of large antenna gain multiplying the Lorentzian tail of the scattered lines. At the same time, if the antenna's bandwidth is narrow enough, and its peak resonance coincides only with the Raman scattering frequency, then there would be little enhancement to the Raman signal. In fact, if we hold the model true, part of the spectral background exhibited in our data at ca 800 cm^{-1} may be related to a real peak.

Fitting for the two antenna types (D- and BT-ant) were obtained with the same gain amplitude $G_0=10.8$, a 15 nm difference in their respective peak resonance and a 35% bandwidth advantage to the D-ant. Key to the model is, therefore a non-linear resonator, which is characterized by its resonance wavelength and its bandwidth regardless of location of the 'hot spot'.

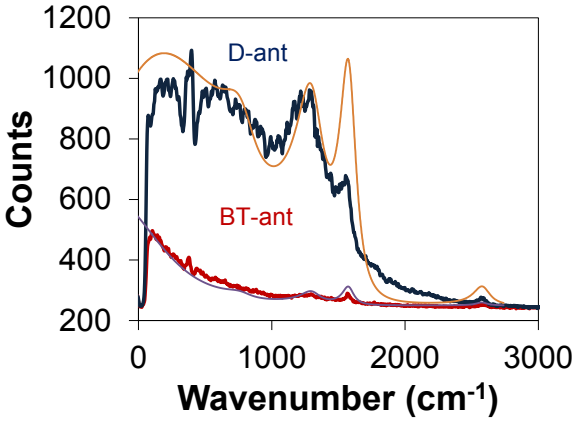

Fig. S2. Fitting Fig.4c: the laser wavelength was 785 nm. The resonance wavelength of the D-ant was taken as λ_0=780 nm (12820 cm^{-1}); the antenna's resonance width was taken as σ_ϖ=4200 cm^{-1}; $\Gamma_1=\Gamma_3=\Gamma_4$=30 cm^{-1}; Γ_2=20 cm^{-1}. A constant spectral background of 250 counts was added to the fit. The BT-ant was simulated with the same Raman line parameters, however with peak antenna's resonance wavelength of λ_0=765 nm (13072 cm^{-1}) and resonance width of σ_ϖ=3100 cm^{-1}. The ratio of Raman amplitudes was 0.02:0.3:1:1 for c_1:c_2:c_3:c_4, respectively. Other common parameters were: a=0.1, G_0=10.8; the graphene density was N=1 and the laser intensity was I_L=1 mW/cm^2.

X-Y scans of integrated peaks: Fitted plots similarly to Fig. 3 are shown in Fig. S3. Area under the peak profile is plotted here instead of the peak value itself.

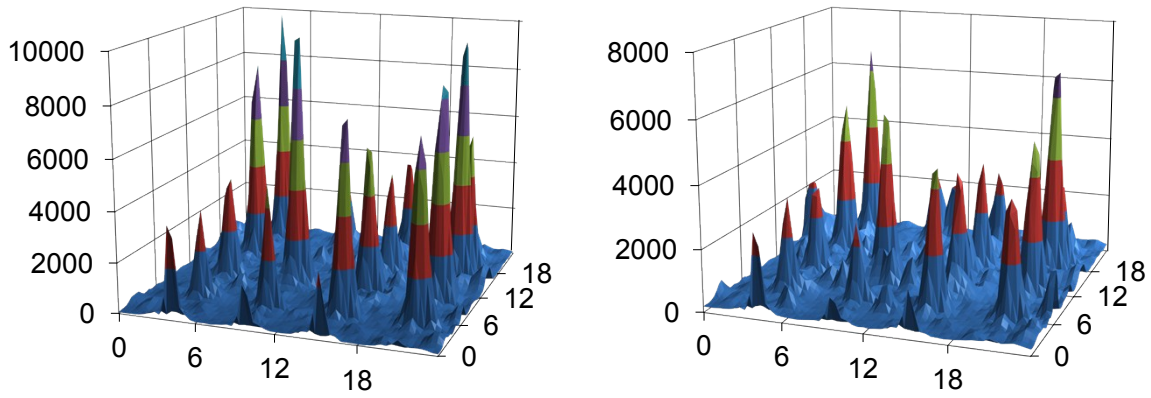

(a) (b)

Fig. S3: Spatial maps for which the spectral background was subtracted: (a) Two-dimensional spatial scan of the integrated D-line. (b) Two-dimensional spatial scan of the integrated G-line. The x and y values are in microns. A 785 nm laser with parallel polarization to the antennas axis was used.

In Fig. S4 we present data for D-ant, which were excited by a 785 nm laser, polarized perpendicularly to the antennas' axis (after the conclusion of scans with the laser polarized parallel to the antenna axis). Here, the integrated peaks became smaller; yet the spectral width of the D and G-lines (Fig. S4c) remained broad. The fiduciary marks became clearer as well. Note that the D- and the G-line were shifted and broadened with respect to reference data obtained in-between the antennas, while the 2D-line was not.

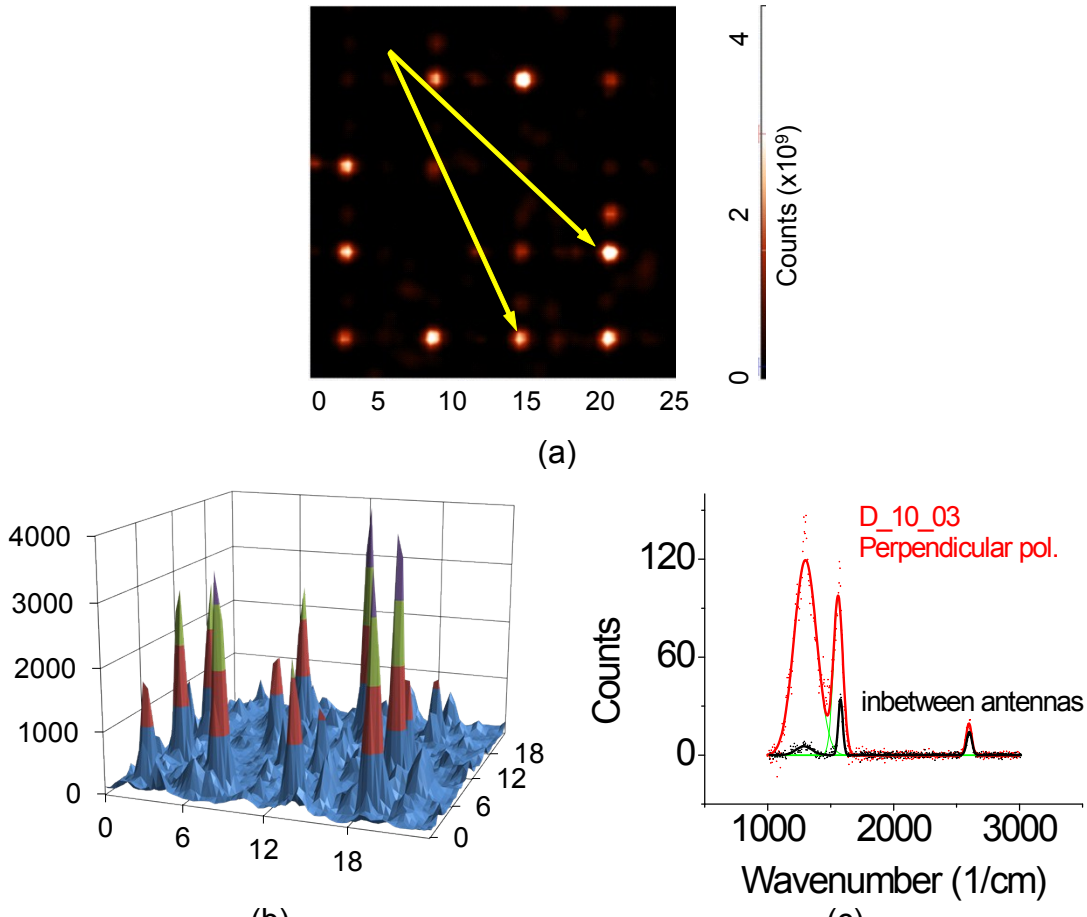

Fig. S4. Using a 785 nm laser, polarized perpendicularly to the antenna's axis after the conclusion of polarized parallel scans. In this case, the antenna is only partially at resonance and the peak values have decreased. The line width has decreased too, by 15%. (a) As-is spatial map of the integrated D-line. The yellow arrows point to some of the antennas. (b) Spectral fitted spatial map of the integrated D-line of graphene. The x and y values are in microns. (c) Spectrum of graphene on a typical antenna and in-between antennas.

As a quick assessment we conducted white light scattering experiments of the samples. Obviously, we averaged here over many antennas and marks. Yet, these experiments convey valuable information about the center scattering wavelength and line widths. The experiments were carried out with a stabilized and collimated white light source (SPEX), a lock-in amplifier (Stanford Research), a spectrometer (SPEX), and a Si detector. The light was focused onto the sample by means of 10x objective. The focused white light spot, with a diameter estimated at 50 μm, covered quite a few antennas and provided for an average reflection signal. The reflection signal from areas with the antennas was normalized by reflection signal from a graphene–coated area without the antennas. In Fig. S5 we show the experimental configuration and the results for 30 nm gap D-ant and 10 nm gap BT-ant, respectively. The signal from the antennas was referenced to the reflection signal obtained for areas without the antennas.

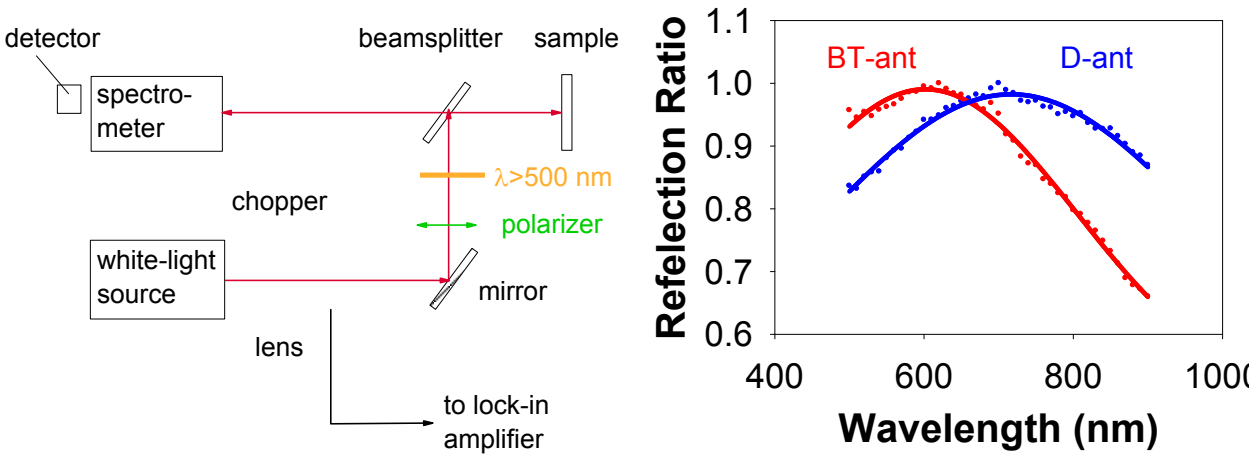

Fig. S5. (a) The configuration for white light experiments. (b) Reflection ratio of 30 nm gap D-ant and 10 nm BT-ant. The reflection signal from the antennas was referenced to the reflection between the antennas. The dots are the experimental data whereas the solid line is a peak fit using a Gaussian distribution. The spectral bandwidth of the D-ant is 0.25 wider than the BT-ant. The incident polarization was parallel to the antenna's axis.

It is clear that the peak reflectance for the BT-ant down shifted to shorter wavelengths, alluding to a larger than expected antenna gap. Upon fitting the white-light data with a Gaussian distribution, we found that the spectral width σ_w for the BT-ant was 200 nm - smaller than the 250 nm spectral width for the D-ant and as anticipated by simulations. Yet, the experimental white-light data indicated larger than expected spectral bandwidth. This may be attributed to the dispersion of the white light source and inhomogeneous broadening by the fiduciary marks in the layout.

In Fig. S6 shows noticeable enhancement and broadening to the graphene D-line, and only small amplification to the G-line when using a 30 nm gap D-ant. There was no red-shift to the Raman lines either.

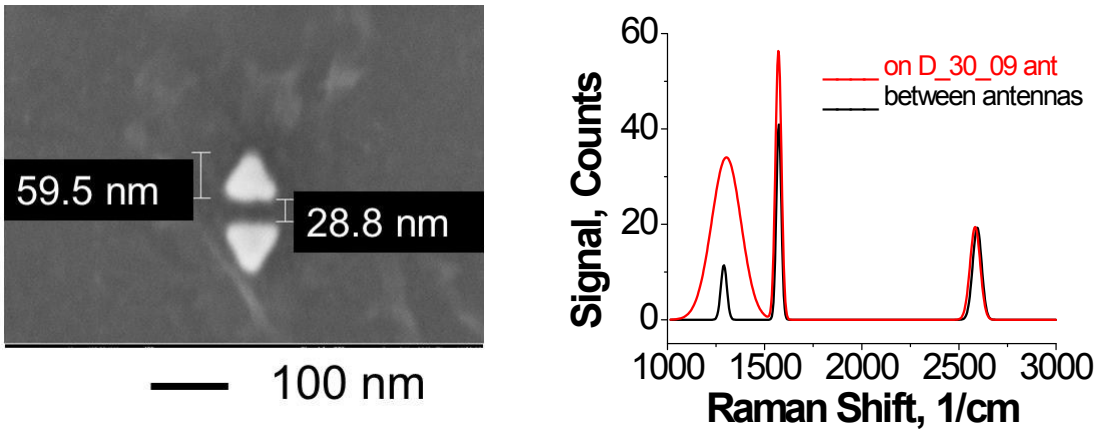

(a) (b)

Fig. S6. (a) SEM picture of a graphene coated D-ant with a 30 nm gap. (b) Fitted spectra of a typical antenna. The laser was 785 nm, polarized parallel to the antennas axis. The laser power was maximal, 28.4 mW, measured just before the objective. Little amplification for the G- and 2D-lines and shift is noted. The importance of measuring the reference signal nearby the antenna is demonstrated by the small but noticeable D-line.

In Fig. S7 we show as-is data for 10 nm BT-ant and D-ant. The 800 cm^{-1} line is easily identified in Fig. S7c yet unresolved in the data from the antenna region. The

spectral background from 0-500 cm^{-1} is attributed to the oxide substrate. Our spectral, background correction curves were presented in the region 1000-3000 cm^{-1} where clear lines could be identified.

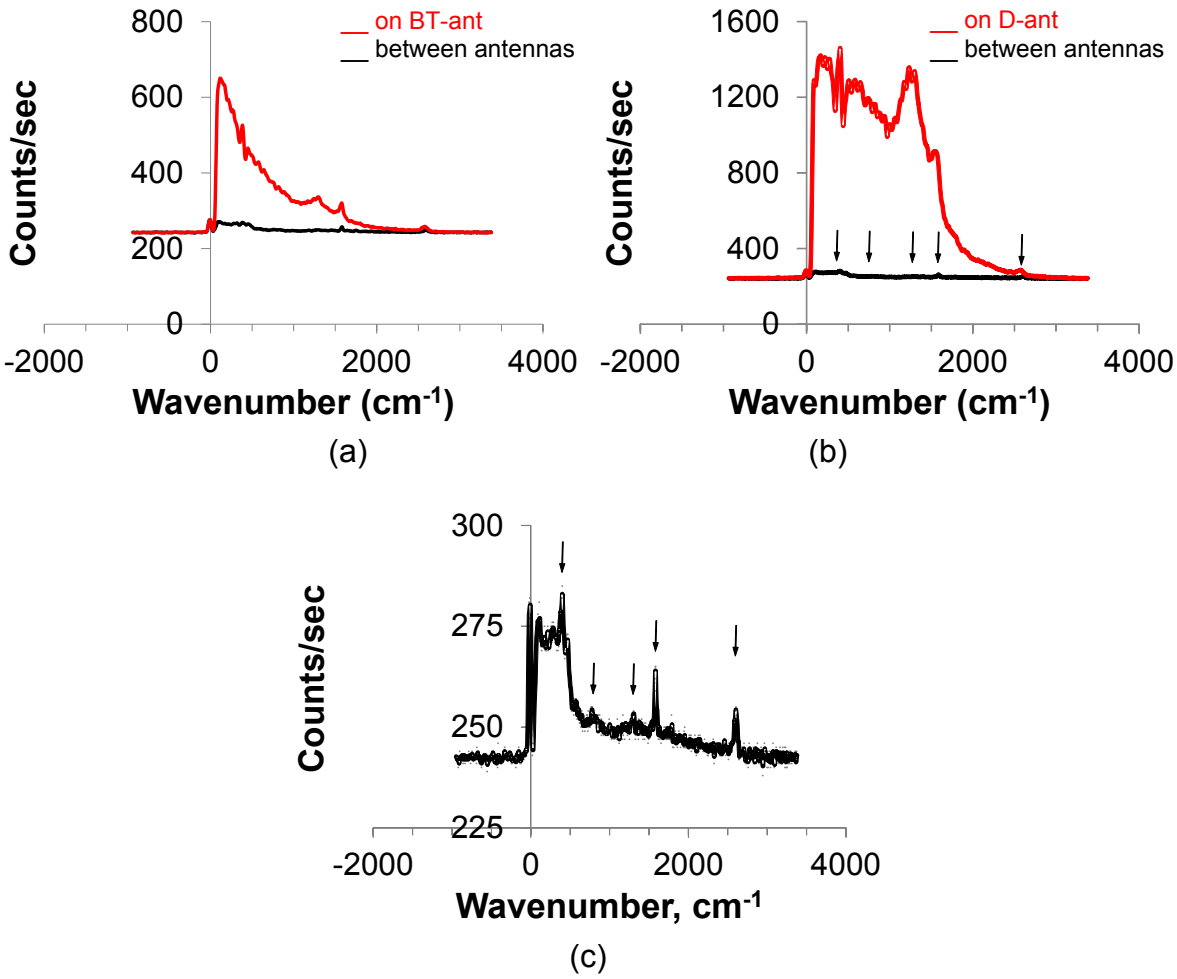

Fig. S7. The entire as-is Raman data for (a) BT-ant (BT_10_09) and (b) D-ant (D_10_09). The arrows in (b) identify the lines at 470 cm^{-1} (oxide), 800 cm^{-1} (amorphous carbon), D-, G- and 2D-lines of graphene. It seems that the G-line is at the gain edge of the D-ant. (c) An expanded view of the signal in-between the D-ant. The positions of the arrows are the same as in (b).

In Fig. S8 we show data upon ramping-up and down the laser intensity through I_L=5.23, 11.64 and 21 mW and back to 5.23 mW. At a given laser intensity, a spatial scan along the axis of the antenna was performed at 400 nm steps across the 4 micron region

about the antenna. Figs S8a,b demonstrate the repeatability of the experiment in terms of peak amplitude and the integrated peak.

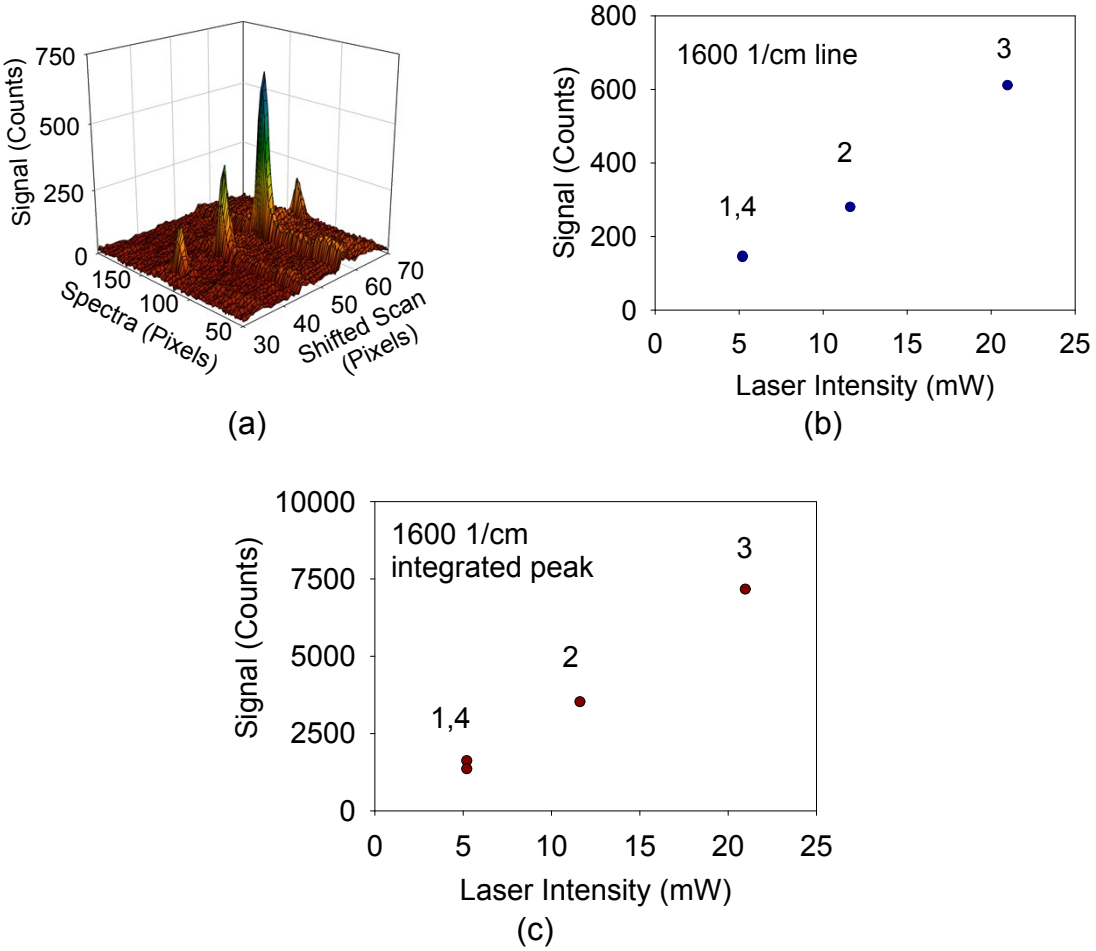

Fig. S8. Intensity plots of the G-line Raman line of graphene. (a) Spectral plots taken at four intensities levels: 1 – 5.23 mW; 2 – 11.64 mW; 3 – 21 mW and 4 – 5.23 mW. The Spectra axis is labeled by pixels of ca 4 cm^{-1} each. Each pixel of the Shifted Scan axis accounts for a 400 nm step. The D-line may be identifies at Spectra~65 for laser level 2,3. (b) Plot of the peak amplitude and (c) plot of the integrated peak signal.

Strain and substrate effects: In Fig. S9 we present data for strained (a) and unstrained (b) graphene on the D-ant. The data were taken from the edge and center of the antennas, respectively. Varying the laser intensity affected the width but not the position of the shifted Raman line. Since the laser spot is larger than the antenna's cross-section,

one may expect signals from the antenna's surroundings, as well. In our case, exciting the antenna at its edge was sensitive enough to detect a shifted Raman line (and thus to strain). As expected, exciting the antenna at its center was more effective in detecting these lines. Due to the small gap between the antenna's elements it is more likely that strain in the graphene film, if present, had been distributed around the antenna along its boundaries and not necessarily at its center. The largest coupling efficiency of the pump beam to the antenna, and hence the generation of plasmonic modes, occurs when the beam is focused at the antenna's center.

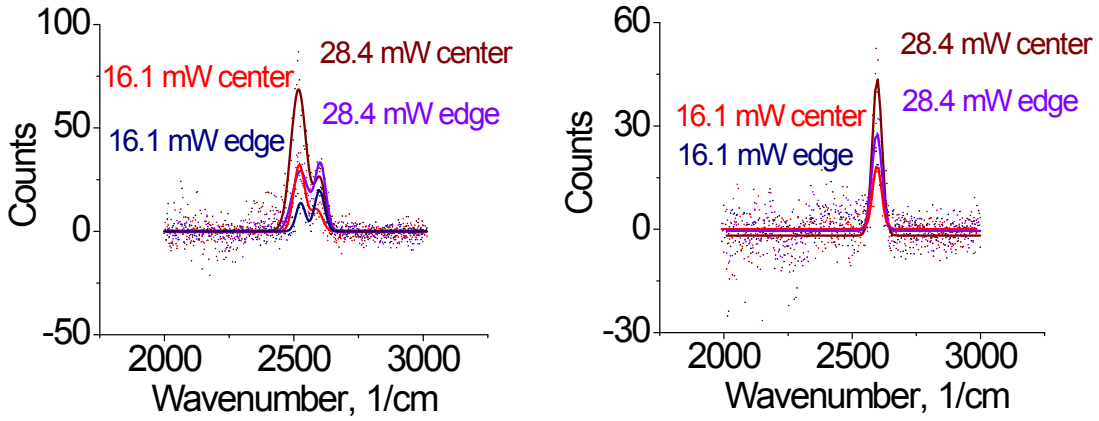

Fig. S9. Strained (a) and unstrained (b) graphene on D-ant. Shown are the 2D lines of graphene on D_10_07 antennas at two pump intensities and at two excitation positions: at the edge or at the center of the antenna, respectively. While both lines in (a) exhibited broadening, the shifted 2D-line was more sensitive to the intensity increase. When exciting the antenna in (a) at the center, there was a small red-shift to the $2D^+$-line at ca 2600 cm^{-1}.

Substrate and strain effects: For the combined effect of strain and surface doping we assume the following linear relationships to the peak shifts: $-\Delta w_G^{(f)}=-\Delta w_G^{(\varepsilon)}+\Delta w_G^{(n)}$ and $-\Delta w_{2D}^{(f)}=-\Delta w_{2D}^{(\varepsilon)}+\Delta w_{2D}^{(n)}$, where positive value is assumed to each shift (thereby, the strain

results in red-shift and the doping results in mostly blue shift of the corresponding line [Ref 46,47 in the main text]. The ratio $\Delta w_{2D}^{(\varepsilon)}/\Delta w_G^{(\varepsilon)}$~2.2 and the ratio $\Delta w_{2D}^{(n)}/\Delta w_G^{(n)}$~0.75. One may convince him/herself that the doping effect will only increase the ratio $\Delta w_{2D}^{(f)}/\Delta w_G^{(f)}$ since the dominator becomes smaller. For reasonable doping level, say, up to 10^{13} cm^{-2}, $\Delta w_{2D}^{(n)}$ is small and the major contribution to the red-shifted 2D-line would be strain. If so, $\Delta w_G^{(\varepsilon)}$ should be always smaller than $\Delta w_{2D}^{(\varepsilon)}$, which is not supported by the data presented in Table 1.

For the optically-induced graphene doping we assume that the loss in the propagating plasmonic mode is translated to an excitation of electron [S1]. In a resonator, the modes are propagating back and forth and endure losses. The life-time of the plasmonic mode in the resonator can be calculated as, $\tau=L/c_n\alpha_L$, where α_L is the loss per resonator pass, c_n is the phase velocity in the antenna resonator and L is the dimension of the resonator (A. Yariv, *Quatum Electronics*). The loss of the propagating mode for a surface mode is, $\alpha=2n\kappa(n_d)^3/[(n^2-\kappa^2)(n_d+n^2-\kappa^2)^3]^{1/2}$ (P.C. Yeh and Yariv, *Optical Waves in Crystals*). Here n_d is the dielectric film covering the metal, n and κ are the real and imaginary refractive values for gold at 785 nm, respectively. For gold antenna [S2], we estimate, α=160 cm^{-1}. The loss per pass is $\alpha_L=\alpha xL$ and τ~0.2 ps, with n_d~1 (the 2 nm alumina covering the gold would not matter much because the wave extends well beyond that layer) and L=150 nm. The life-time of the plasmonic mode is increased by the Q~10 factor of the resonator so τ_{eff}=2 ps [S3]. We also assume that the plasmonic mode propagates mostly in air and the antenna is occupying only 0.046 of the spot size area.

As a limiting case we assume that the generated carriers in the metal are all used in the doping of graphene. The number of electrons generated in the gold antenna by

the 20 mW laser and focused into 0.7x0.7 micron^2 spot-size is: $G=(r)(\alpha_L Q)(I_{in}/h\nu)$. Here r is the antenna area to spot-size ratio, $\alpha_L Q$ is the overall loss of the propagating plasmonic mode, and $I_{in}/h\nu$ is the density of electrons in cm^{-2}. G~0.2x10^{23} cm^{-2}. At steady states, $G-n_1/\tau=0$, where τ is the electrons life-time. With τ=2 ps, the density of the optically generated electrons n_1 is G/τ or, n_1=4x10^{10} cm^{-2}. In general, $V-V_0=(E_f/e)-e*n*(\text{Area})/C$. Here, V is the applied bias to the electrode (antenna), V_0 is the surface potential, $C=\varepsilon*(\text{Area})/d$ is the geometric capacitor formed between the antenna and graphene across the d=2 nm alumina layer with a dielectric constant of $\varepsilon\sim5\varepsilon_0$; $n=n_0+n_1$ is the total density of electrons (including environmental doping effects, such as water vapors). The change in the Fermi energy due to optical doping is, $\Delta E_f=e^2*n_1*d/\varepsilon$ in Joules. We estimate that ΔE_f~3 meV.

Methods

Antennas layout and fabrication. Ti/Au (3 nm/17 nm) nano-antennas were fabricated on 4" quartz wafers using e-beam lithography. These were of diamond shape (D-ant) and bowtie (BT-ant), with three gap values of 10, 20 and two 30 nm for the D-ant and 5, 10 and two 20 nm for the BT-ant. Approximately 500 antennas were fabricated for a given gap value and dose; nine e-doses were used; in total there were ~4500 antennas per given gap value, albeit variation in antennas efficiency is noted (see SI section Figs. S3, S4). It was initially expected that the antennas would not be easily identified so we included fiduciary marks to the antenna layout. These were placed 2 μm away from each antenna. The marks were either rectangular (100 x 300 nm) or disk (100 nm in diameter) shapes and were made of Ti/Au (3nm/17 nm). The upper gold surface was coated with

2 nm thick amorphous Al_2O_3 film using atomic layer deposition (ALD), thus separating the conductive graphene from the antenna; in this way we eliminated the chemical enhancement contribution to the Raman signal, as well.

Graphene CVD deposition. Graphene layers were grown in an Aixtron "Black Magic" system on 4", 25 μm copper foils (Sigma-Aldrich) and were transferred onto the antenna layout. The transfer was completed by first depositing a layer of 300 nm thick poly(methyl methacrylate) (PMMA) and subsequently etching the copper foil by $FeCl_3$ [S3]. The PMMA film was later removed by immersing the samples in acetone.

Spatial and spectral scans. NT-MDT Raman system in confocal mode was used with a 30 mW 532 doubled Nd:YAG laser, a 30 mW 633 nm HeNe gas laser and a 70 mW 785 nm semiconductor laser. The laser intensity at the sample has decreased by more than 10 dB of that value because of fiber coupling, filtering and scattering. The maximum laser intensity, measured before the x100 objective was ca 28 mW for the 785 nm laser. The system was equipped with a translational stage which maintained 2-nm accuracy for over 2 hours. The laser beam was focused before every scan and its focusing after the scan was ascertained by on-axis CCD camera. The spectrometer was equipped with a cooled Si CCD array (Andor). Spectrometer gratings were 600 grooves/mm (blazed at 600 nm) when using the 633 nm and the 532 nm lasers and 150 grooves/mm (blazed at 500 nm) when using the 785 nm laser. The latter grating accommodated the wide spectral range of Raman scattering associated with the 785 nm laser and its line width of 0.5 nm. We note that the broadening of the Raman lines were real: it exceeded the laser line

width by far. The 2D graphene line was situated at λ=985 nm when excited with the 785 nm laser, fairly close to the Si-based, camera's sensitivity edge. We used an achromatic 100x objective lens (NA 0.7) to focus the laser beam onto the sample. Data accumulation times for each point were 0.5 s for the 633 nm and 532 nm lasers and 1 and 2 s for the 785 nm laser. SEM pictures taken after laser scanning ascertained that the antennas were not damaged during the experiments (e.g., Fig. S6).

Simulations and spectral analysis. Commercial COMSOL code was used to simulate the various structures. The simulated full structure consisted of a quartz substrate, metal, a 2 nm Al_2O_3 film, two layers of suspended graphene. Spectral fitting and subtration of spectral background were made by using two routines: one was provided by the NT-MDT system software and the other was ours, based on a MathWorks background correcting module. Both codes gave similar results regarding the peaks value and its width.

[S1] Anneli Hoggard et al, "Using the Plasmon Linewidth to Calculate the Time and Efficiency of Electron Transfer between Gold Nanorods and Graphene", ACS Nano, December 23, 11209–11217 (2013). doi:10.1021/nn404985h

[S2] M. A. Ordal, L. L. Long, R. J. Bell, S. E. Bell, R. R. Bell, R. W. Alexander, Jr., and C. A. Ward, "Optical properties of the metals Al, Co, Cu, Au, Fe, Pb, Ni, Pd, Pt, Ag, Ti, and W in the infrared and far infrared", Appl. Opt. 22, 1099-1119 (1983).

[S3] K J Tielrooij, M Massicotte, L Piatkowski, A Woessner, Q Ma, P Jarillo-Herrero, N F van Hulst and F H L Koppens, "Hot-carrier photocurrent effects at graphene–metal interfaces", J. Phys.: Condens. Matter, 27, 164207 (2015)

[S4] Xuesong Li, Yanwu Zhu, Weiwei Cai, Mark Borysiak, Boyang Han, David Chen, Richard D. Piner, Luigi Colombo and Rodney S. Ruoff, “Transfer of Large-Area Graphene Films for High-Performance Transparent Conductive Electrodes”, Nano Letts, 9(12), 4359-4363 (2009).